Studies on Physicochemical, Biological and Antibacterial Application of Silicon Dioxide (SiO_2), Tricalcium Silicate (Ca_3SiO_5) and a Composite with Calcium Silicate Materials

A.Z. Sayyed[1], A.M. Patil[2]
[1,2]*Department of Physics, R. C. Patel Arts Commerce and Science College, Shirpur-425405, India*
doi.org/10.64643/IJIRTV13I2-206285-459

***Abstract*— This study investigates the synthesis, characterization, and biological evaluation of silicon dioxide (SiO_2), calcium silicate (Ca_3SiO_5) and a composite with calcium silicate (SiO_2/Ca_3SiO_5). Silicon dioxide nanoparticles were synthesized using the Stöber method and the C3S was synthesised by sol-gel technique. Synthesised materials were characterized by standard state-of-the-art technologies for structural and phase analysis such as X-ray diffraction (XRD) and Raman spectroscopy, respectively. Biological evaluation included bioactivity assessment through simulated body fluid (SBF) immersion and antibacterial testing against Escherichia coli and Staphylococcus aureus. SiO_2/C3S achieved exceptional bioactivity (95% HA coverage at 21 days), compared to the bare materials.**

***Index Terms*— silicon dioxide, calcium silicate, antibacterial activity, bioactivity, SiO_2, Ca_3SiO_5**

I. INTRODUCTION

The defects of bones are due to the tumour and abnormal skeletal development leads significant dysfunction and disability.[1] This issues are major which needs the approach that combines the clinical advancements and research.[2] The research of hybrid nanocomposite nanomaterials for, which include organic and inorganic materials have gained an immense interest for mutli-applications, one of the major applications include antibacterial and other bioactive fields.[3] The properties of the hybrid composites have mostly improved the performance with strategic compositions and elements.[4] The calcium silicate and silicon oxide has gained the interest of researchers due to its facile synthesis, cost-effectiveness, bone repair, and bioactivity.[5,6] Calcium silicate and silicon oxide enhances the pH in localized environment, making these materials potential and applicable in bioactivities. However, increase in the localized pH contributes to antibacterial activity, helping the bon generation and repair. Thus the researchers are actively engaged in in the exploration of antibacterial and osteogenic applications.[7–10] Ming-Cheng lin, et al. reported the enhanced antibacterial activity of sol-gel synthesized calcium silicate and hybrid materials for bone repair.[11] Joelle El Hayek, et al. reported the 3D printed silver nanoparticle functionalized calcium silicate ceramics for antibacterial applications.[12] Yang-Xuan Hou et al. studied SiO_2 for antibacterial applications and a comparison with the combination of Ag, Cu, Ce, and Ni based oxides under dark and illuminated conditions.[13] Yanxia Zhang et al. studied the SiO_2 coated ZnO for antibacterial applications in bone repairs.[14] The calcium silicate and silicon based composite materials were reported intensively for antibacterial and osteogenic applications.

The enormous properties of silicon oxides and calcium silicates for antibacterial and osteogenic applications.[15–17] The Ca_3SiO_5 and SiO_2 can be synthesized by hydrothermal, sol-gel, co-precipitation, etc.[11,18–20] One of the most feasible and const-effective techniques to synthesize Ca_3SiO_5 and SiO_2 are sol-gel method and stable Stöber methods, respectively.[21–23] Therefore, the sol-gel synthesized Ca_3SiO_5 and Stöber method based synthesized SiO_2 were studied for antibacterial and osteogenic applications with the state-of-the-art advanced techniques. The structural analysis for both materials was analyzed by X-rya diffraction method and phase analysis was determined

by Raman spectroscopy. The morphological properties were studied by scanning electron microscopy. Furthermore, the bare Ca_3SiO_5 and SiO_2 were used for biological responses, including MG-63 and antibacterial activities were studied with E. coli and S. aureus.

II. EXPERIMENTAL SECTION

2.1 Materials: Tetraethyl orthosilicate (TEOS, 99%), calcium nitrate tetrahydrate (Ca $(NO_3)_2 \cdot 4H_2O$, 99%), sodium hydroxide (NaOH, 98%), ammonia solution (NH_3, 28-30%), and ethanol (99.9%) were purchased from Sigma-Aldrich. All reagents were of analytical grade.

2.2 Synthesis Methods

2.2.1 Synthesis of Silicon Dioxide (SiO_2)

Amorphous SiO_2 was synthesised by the stable Stöber method.[24] A mixture containing 100 mL ethanol, 10 mL deionized water, and 5 mL ammonia solution (28%) was prepared in a round-bottom flask under magnetic stirring at 25°C, 500 rpm for 15 minutes. Subsequently, 8 mL of TEOS was added dropwise. Hydrolysis and condensation proceeded for 6 hours. Particles were collected by centrifugation at 10000 rpm for 15 minutes, washed three times with ethanol and twice with deionized water, dried at 100°C for 12 hours, and calcined at 600°C for 3 hours. As synthesized materials was used for further characterizations.

2.2.2 Sol-gel Synthesis of Ca_3SiO_5 (C3S)

The synthesis of Ca_3SiO_5 (C3S) was carried out by cost-effective sol-gel technique.[25–27]Calcium nitrate tetrahydrate (11.81 g, 50 mmol) was dissolved in 150 mL ethanol-water mixture (2:1 v/v). TEOS (10.42 g, 50 mmol) was added dropwise, pH maintained at 11.0. The sol was stirred at 60°C for 4 hours, aged 72 hours, dried at 120°C for 24 hours, and calcined at 700°C for 5 hours. As synthesized materials was used for further characterizations. The collected C3S powder was then physically combined with SiO_2 with distinct ratios, for enhanced activity study. The physical composites were prepared with distinct weight ratios.

III. RESULTS AND DISCUSSION

3.1 Structural, Phase and Morphological Analysis

To determine the structural properties of synthesized SiO_2 and Ca_3SiO_5 materials, X-ray diffraction (XRD-Cu Kα) spectroscopic measurements were carried out. Figure 1 (a) shows the XRD pattern of amorphous SiO_2 with affirmative broad peak at 22.03º. The broad peak observed for silicon oxide may be due to the smaller size, which demonstrates that a high percentage of the SiO_2 particles are amorphous.[28] Figure 1 (b) shows the Raman spectra of SiO_2 in which the peaks observed at 434, 495 (D1), 604 (D2), 799, 1075 ($T_2(F_2)$), and 1081 (A_1) cm^{-1} wavenumbers.[29] The peak at asymmetric band at 434 corresponds to rocking Si-O-Si bonds, and 1081 (A_1) corresponds to symmetric stretching Si-O-Si bonds associated with SiO_4 tetrahedra. The D_1 band refers to symmetric stretching of oxygen, and D_2 band refers to breathing modes of oxygen. The band at 799 corresponds to Si motions within the tetrahedrals of oxygens and T_2 (F_2) & A1 modes corresponds to an isolated SiO_4 tetrahedron with T_d symmetry.[29] Figure 1 (c) shows the XRD patter of C3S with the peaks and the corresponding planes observed are 23.33 (021), 24.90 (131), 29.53 (132), 31.12 (122), 32.66 (230), 34.35 (212), 37.49 (240), 39.7 (312), 41.39 (331), 42.39 (400), 44.62 (303), and 46.40 (152).[30,31] The crystalline size for C3S was evaluated for the peak positioned at (230) plane by scherrer equation. The crystalline size was evaluated to be 10.90 nm for Ca_3SiO_5 (C3S).[32,33] To analysis of the phase based evaluation was carried out by Raman spectra for C3S, shown in Figure 1 (d). The Raman spectroscopy was carried out in in the range of 150 to 1500 cm^{-1} for C3S. The high frequency region of the Raman spectra, ranging from 800 to 100 cm^{-1} is a diagnostic region, corresponding to the symmetric stretching of Si-O. Observed the multiple peaks corresponds to the symmetric Si-O stretching caused due to non-equivalent cyrtsallographic sites. The affirmative region around ~250 cm^{-1} is the region of Ca-O vibrations and OH translation in the region of ~380 cm^{-1} corresponding to surface hydration.[34]

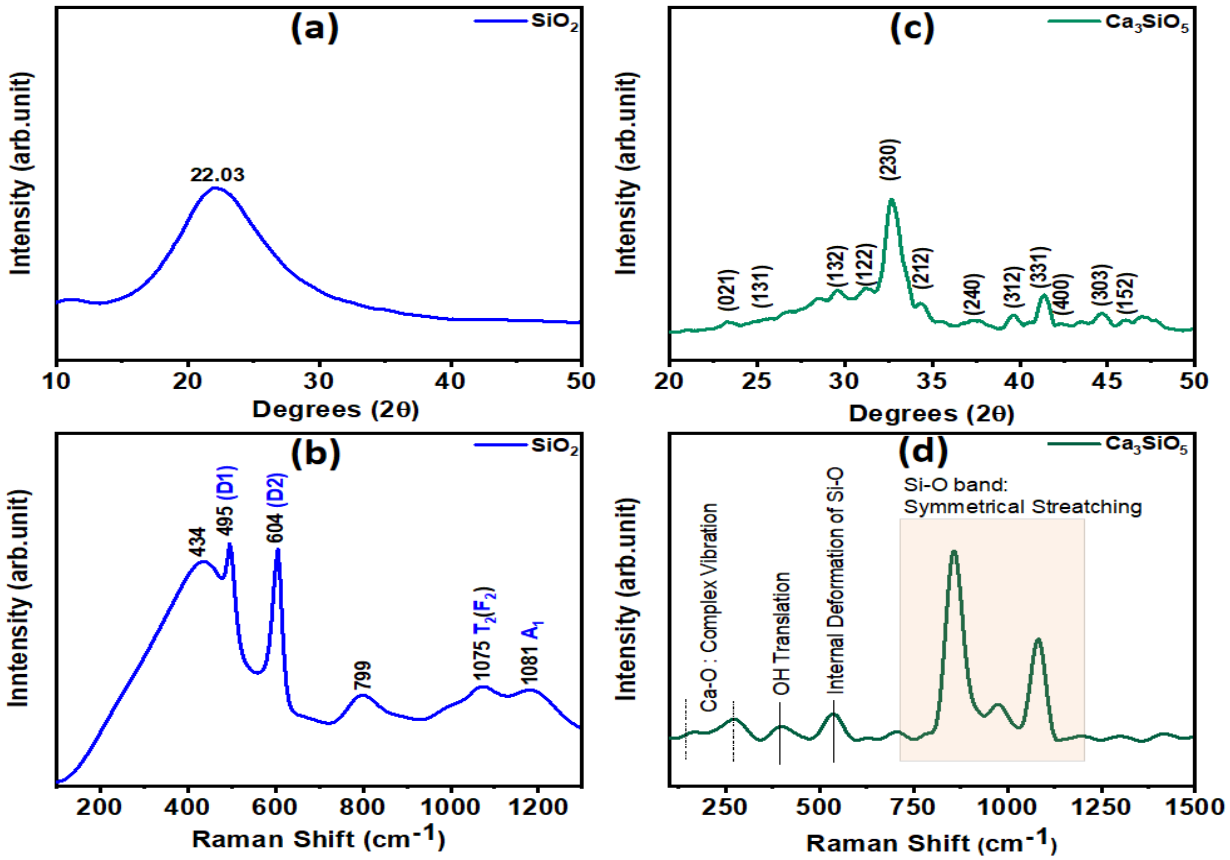

Figure 1. (a) XRD and (b) Raman spectra of SiO_2. (c) XRD and (b) Raman spectra of Ca_3SiO_5.

Figure 2 (a, b) shows the scanning electron microscopic images of SiO2 and C3S materials. The magnification at which the SEM images observed for SiO2 and C3S, were at 5000x and 2000x, respectively. For the both the materials, SEM images show bulk and non-uniform agglomerations with some whiskers.

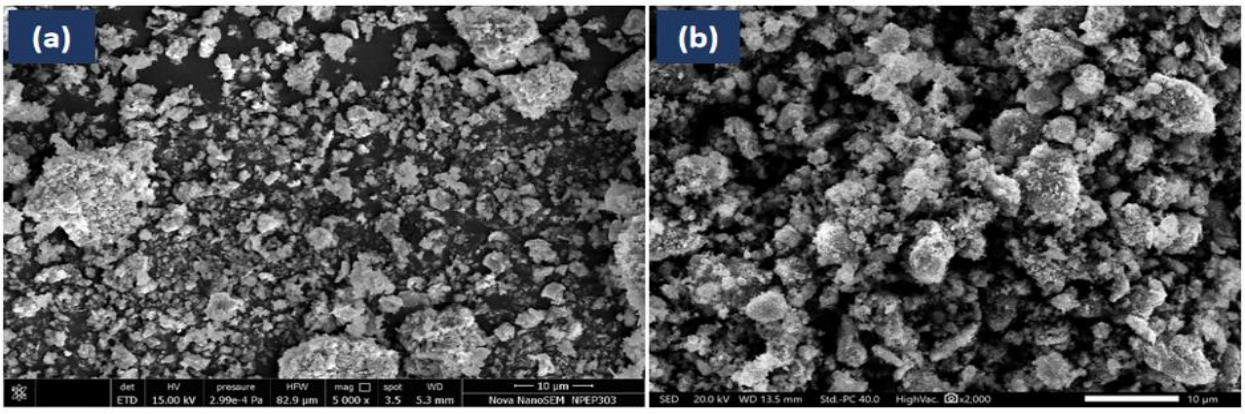

Figure 2. Scanning electron microscopic images of (a) SiO_2 and (b) Ca_3SiO_5 (C3S).

3.2 Bioactivity Assessment-

3.2.1 Optimization SiO_2/C3S Composite:

To determine the optimal ratio of C3S and SiO_2 for high bioactivity or antibacterial efficacy, the localized pH rise over time was observed under the condition of immersed materials in neutral aqueous medium (room temperature). The distinct ratios of C3S and SiO_2 was prepared, as shown in Figure 3 (a) for distinct ratio such as 100, 80, 60, and 30 percent of C3S and 20, 40, 70 and 100 of SiO_2 materials as physical composites.

The resulting kinetic curves shown in Figure 3 (b), reveal distinct behavioural zones that dictate how the material interacts with bacteria and surrounding living tissues. The most pathogenic bacterial (E. coli and S.aureus) cannot survive when the ambient pH shifts and stabilizes above 10.5 to 11. The pure C3S (0% SiO_2) overshoots thus threshold rapidly, climbing toward 12.5 of pH. While highly antibacterial response, this harsh alkaline nature can damage osteoblast stress and cause severe stress during application. The 80:20 composite acts as a self-buffering system, as the initial dissolution of C3S rises the pH, but the 20% of amorphous SiO_2 actively participates and helps maintaining moderate pH11.4 - 11.5. This maximizes bacterial eradication while maintaining a more biocompatible system. The ratios above 40% of SiO_2 fail to sustain the high pH threshold over 11 across extended periods due to the abundant silica acting as a chemical sink.

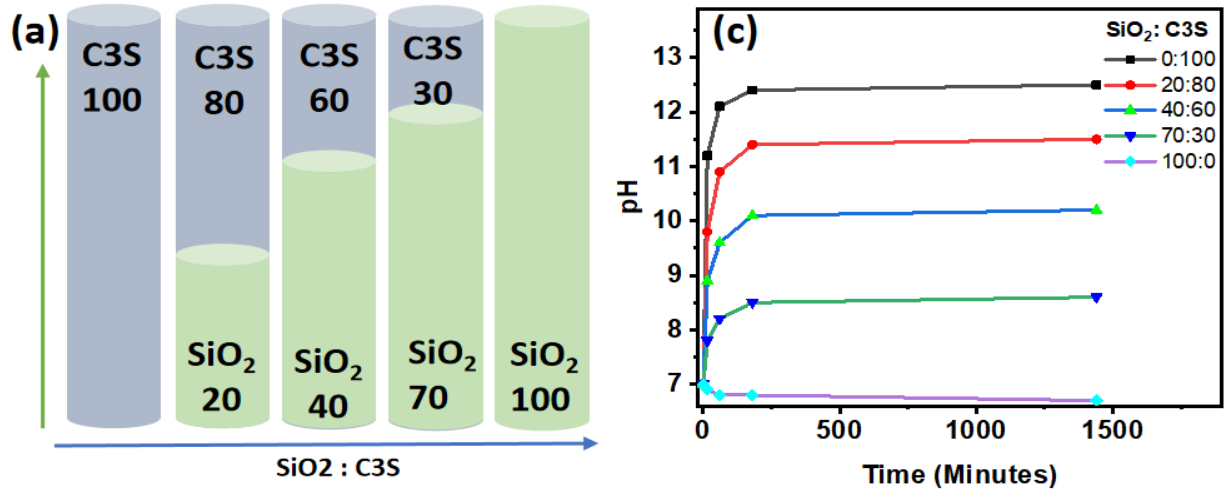

Figure 3. (a) SiO2 vs C3S physical composite ratio and (b) change in pH vs Time (mintes) plot for SiO_2 and C3S composite of distinct ratios.

3.2.2. Hydroxyapatite Formation

Samples immersed in SBF (pH 7.40, 37°C) prepared per Kokubo & Takadama. HA formation assessed at 3, 7, 14, and 21 days. Figure 4 (a) tracks the percentage of the material's surface covered by bone like hydroxyapatite over 21 days. The composite SiO_2/C3S drastically outperforms both pure C3S and pure SiO_2. By day 7, the composite already exhibits ~70% coverage, compared to ~50% for C3S and ~35% for SiO_2. Bioactivity requires two main things, a source of Calcium (Ca^{2+}) and Phosphate (PO_3^{3-}) ions, and surface nucleation sites to lower the thermodynamic barrier for crystallization. Pure SiO_2 provides abundant silanol groups (Si-OH) on its surface when hydrated. These are excellent, negatively-charged nucleation sites, but pure silica lacks an internal calcium source, making HA precipitation slow. Pure C3S releases massive amounts of Ca^{2+} into the fluid, rapidly super-saturating the local environment, but it has fewer stable silanol nucleation sites initially. The composite SiO_2/C3S combines both advantages. The C3S acts as a calcium source releasing Ca^{2+} ions, while the SiO_2 phase provides a dense network of silanol nucleation sites. The Ca^{2+} ions are immediately electrostatically attracted to the Si-O^- groups on the silica phase, creating a highly favorable interface for instantaneous apatite nucleation. The bioactivity of the SiO_2, C3S and SiO_2/C3S. SiO_2 showed good bioactivity with HA peaks appearing at 7 days, reaching 65% surface coverage by 21 days (pH increased to 7.72), driven by dissolution of surface Si-OH groups promoting calcium phosphate nucleation from SBF. C3S demonstrated excellent bioactivity: HA peaks were clearly visible at 3 days, reaching 87% coverage at 21 days with HA layer thickness of 2–4 µm and pH 7.95. SiO_2-C3S exhibited the best bioactivity among all materials tested: 45% coverage at 3 days, 70% at 7 days, 90% at 14 days, and 95% surface coverage with a 3–5 µm HA layer at 21 days (pH 7.88). The SiO_2 component contributed abundant silanol groups acting as nucleation sites.

Figure 4 (b) shows the pH rise of the SBF solution, which originally starts at physiological pH (7.40). (Note: Because SBF is a buffered solution, the pH does not shoot up to 12 like it does in pure water, but the relative differences are highly informative). Pure C3S causes the highest pH rise (reaching ~7.95). Pure SiO_2 causes the lowest pH rise (~7.72). The SiO_2/C3S composite sits perfectly in the middle (~7.88). When C3S hydrates, it undergoes a highly alkaline reaction, releasing calcium hydroxide Ca (OH)2 and forcing a sharp rise in pH. When SiO_2 is added to form the composite, it acts as a chemical buffer through a pozzolanic reaction. The amorphous silica network reacts with the excess OH^- and Ca^{2+} released by the C3S to form a stable Calcium-Silicate-Hydrate (C-S-H) gel.

Pure C3S releases plenty of ions, but its higher pH and rapid dissolution can cause surface instability, slightly hindering maximum HA formation. Pure SiO_2 is structurally stable but chemically too slow. The SiO_2/C3S composite creates an effective environment: the pH is alkaline enough to trigger structural breakdown and possibly offer mild antibacterial resistance, but buffered enough by the silica to maintain an ideal, stable surface for cells and minerals. Consequently, this regulated ion exchange and high density of silanol groups result in the fastest, most comprehensive hydroxyapatite formation.

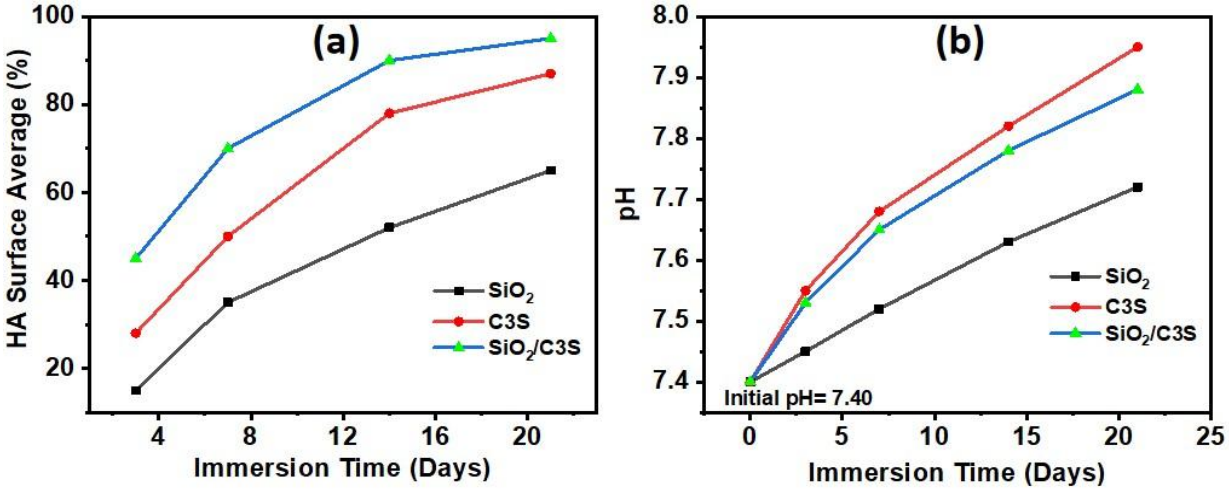

Figure 4. Bioactivity assessment in simulated body fluid (SBF). (a) Hydroxyapatite (HA) surface coverage (%) vs. immersion time and (b) pH changes of SBF solution during immersion.

3.2.3 Antibacterial Activity

Antibacterial activity for SiO_2, C3S, and SiO_2/C3S was carried out against E. coli (ATCC 25922) and S. aureus (ATCC 25923) using disk diffusion (Mueller-Hinton agar, 37°C, 24h), colony counting (CFU/mL), and MIC determination (broth microdilution, 96-well plates). Figure 5 (a, b, c, d) presents a comprehensive microbiological evaluation of pure SiO_2, pure C3S, and the SiO_2/C3S composite against two standard pathogenic models: E. coli (Gram-negative) and S. aureus (Gram-positive). Figure 5 (a), the zone inhibition assay provides a macro-level look at how well the antibacterial agents (dissolved ions) travel through an agar medium. The 6mm dashed line corresponds to the physical boundary of the test disk; anything at this line implies zero inhibition beyond physical contact. Pure SiO_2 acts as a near-inert control here, barely clearing the 6mm baseline. While pure C3S generates a clearance zone (~9-10.5mm), the composite formulation significantly extends this radius (reaching ~12mm against S. aureus). This suggests that the composite matrix facilitates a more efficient, continuous diffusion of active ions into the surrounding environment compared to the pure silicate. Figure 5 (b), the MIC data isolates the intrinsic potency of the materials. Lower values indicate a stronger material. It is observed that, the synergetic effect of the composite SiO_2/C3S is SiO_2/C3S outperformed the bare materials. Against S. aureus, the composite requires an MIC of only 250 µg/mL. To achieve the same effect of composite, the concetration of C3S will be required double than SiO_2/C3S (500

µg/mL), and a massive 8-fold increase of SiO_2 (2000 µg/mL). Figure 5 (c), corresponds to the previous studies, showing the total percentage of bacterial death over a 24-hour period. The composite achieves the highest mortality rates across both bacterial strains, confirming that the larger inhibition zones and lower MICs translate directly to higher absolute kill rates in a liquid culture medium.

Figure 5 (a) shows the antibacterial activity of SiO_2, C3S and SiO_2/C3S materials against E. coli and S. aureus with inhibition zones. The baseline disc size of 6mm was used. Figure 5 (a, b) present the antibacterial response against E. coli and S. aureus. SiO_2 showed minimal antibacterial activity (zones: 7.5 ± 0.5 mm for E. coli, 8.2 ± 0.6 mm for S. aureus; MIC >2000 µg/mL). C3S resulted in moderate activity (zones: 9.2 ± 0.6 mm / 10.4 ± 0.7 mm; 24h reduction: 42.8% / 48.6%; MIC: 1000 / 500 µg/mL), mainly from the calcium silicate component. Sol-gel SiO_2/C3S resulted in enhanced activity (zones: 10.8 ± 0.7 mm / 12.1 ± 0.8 mm; 24h reduction: 48.5% / 54.2%; MIC: 500 / 250 µg/mL) compared to the bare SiO_2 and C3S, attributed to its higher surface area enabling greater ion release.

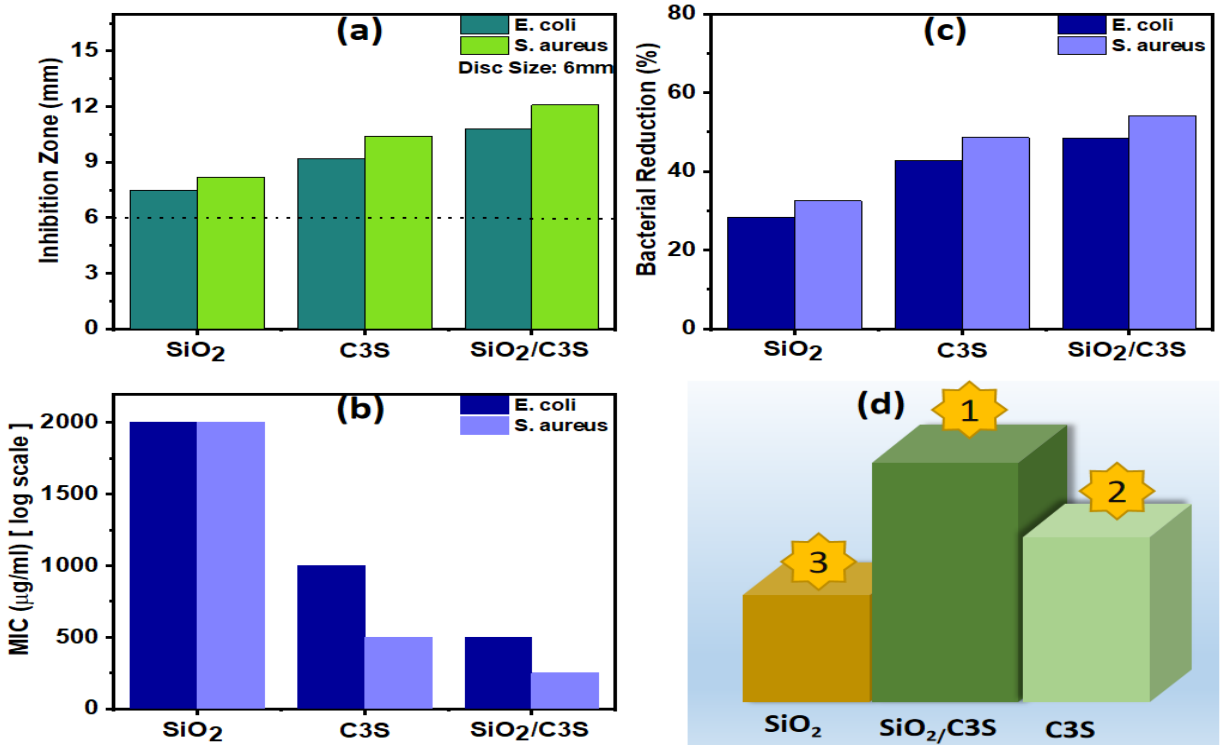

Figure 5. (a) Inhibition zone diameter (disk diffusion); (b) Minimum inhibitory concentration (MIC, µg/mL, log scale); (c) 24h bacterial reduction (%). Dashed line in (a) = disk diameter (6 mm).

IV. TIME DEPENDANT ANTIBACTERIAL STUDY

The time-dependent antibacterial efficacy and differential susceptibility profile of the synthesized SiO_2, C3S and composite SiO_2/C3S materials are illustrated in Figure 6 (a, b). To evaluate the kinetic behaviour of the antibacterial action, bacterial reduction was monitored at two distinct time intervals: a short-term incubation of 4 hours and an extended exposure of 24 hours as shown in Figure 6 (a).

For both C3S and SiO2/C3S samples, a distinct time-dependent increase in bactericial activity was observed against both E.coli and S.aureus. It has been observed that E. coli reduction of 34.5% at 4 hours, which significantly progressed to 42.8 after 24 hours. A parallel trend was noted against S. aureus, where the reduction capacity intensified from 39.0% to 48.6% over the same period. This continuous increase in antimicrobial efficacy over time indicates a sustained release mechanism of active therapeutic species—likely silicone- and calcium-based ions—from the

silicate matrix, ensuring prolonged contact-killing and membrane disruption without premature saturation. When comparing the C3S and its composite SiO_2/C3S, the SiO_2/C3S matrix consistently outpaced its bare counterparts across all time points. The SiO_2/C3S sample achieved a remarkable 54.2% reduction of S. aureus and 48.5% reduction of E. coli at the 24-hour mark. This enhanced performance can be attributed to the inherent structural advantages of the SiO_2/C3S, which typically yields higher specific surface areas, finer nanoscale porosity, and a more uniform distribution. These structural features optimize the interfacial contact between the material and the bacterial cell wall, accelerating the accumulation of localized oxidative stress or ionic disruption. To further understand the mechanistic pathways governing these interactions, Figure 6(b) display the comparative susceptibility between Gram-negative (E. coli) and Gram-positive (S. aureus) strains after 24 hours of exposure. In the SiO_2/C3S composite, the reduction rate transitions from 48.5% for E. coli to 54.2% for S. aureus. This differential susceptibility is supported by the fundamental structural variations in the bacterial cell envelopes. Gram-negative E. coli possesses a highly complex, chemically restrictive outer lipid membrane that acts as an effective asymmetric barrier against the diffusion of foreign ions and reactive species into the intracellular environment. Conversely, the cell wall of Gram-positive S. aureus, while thick, is composed of a porous peptidoglycan network that lacks this outer lipopolysaccharide membrane. Consequently, the cell wall of S. aureus is considerably more permeable to the released silicate/calcium ionic species and associated reactive oxygen species (ROS), leading to more direct intracellular penetration, cellular leakage, and metabolic collapse. This analysis underscores that while fabrication parameters like the SiO_2/C3S process can optimize the properties of the materials, the ultimate bactericidal throughput remains inherently governed by the structural biology of the target pathogen.

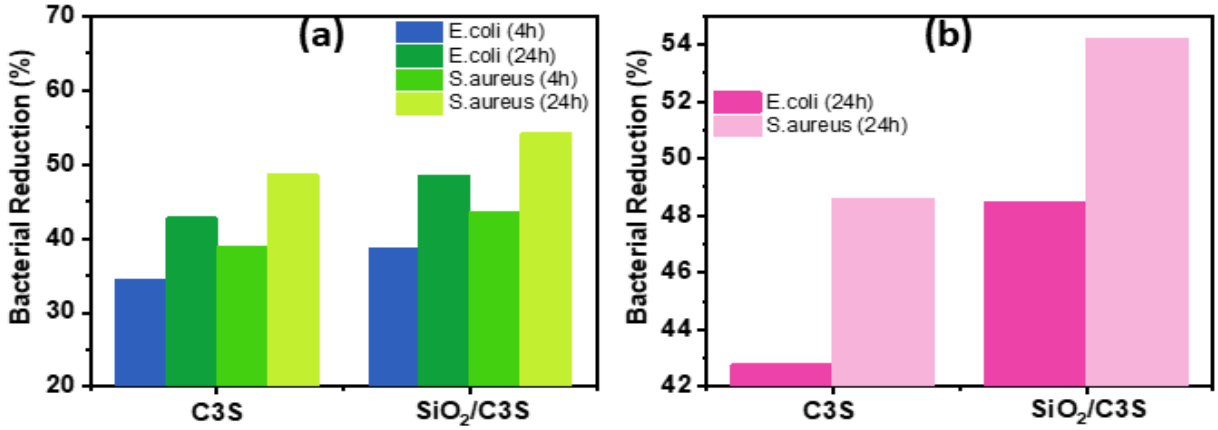

Figure 6. (a) Time-dependent bacterial reduction comparing 4h and 24h incubation periods, (b) Comparison of Gram-negative E. coli vs. Gram-positive S. aureus susceptibility at 24h.

V. MECHANISM

Sustained vs Passivated ion Release:

Upon exposure of C3S is exposed to an aqueous environment, it reacts violently, rapidly releasing Ca^{2+} and OH^- ion. However, this hyper-reactive surface quickly precipitates a dense, impermeable Calcium-Silicate-Hydrate (C-S-H) gel layer on its own surface. This passivation layer traps unreacted material inside, effectively choking off further ion release after the initial burst. Bacteria that survive the initial alkaline shock can eventually recover. Integrating the SiO_2 network alters the hydration kinetics. The silica acts as a structural disruptor and chemical buffer, preventing this dense passivation layer from sealing the surface. Instead of a massive, short-lived alkaline spike, the composite provides a sustained, steady-state release of hydroxyl ions over a prolonged period. Prolonged environmental alkalinity induces continuous osmotic stress and gradual membrane saponification, which is far more lethal to bacterial colonies over a 24-hour window.

Gram-Positive vs Gram- Negative Vulnerability:

A consistent trend across all three empirical graphs is that S. aureus is notably more susceptible to the biomaterials than E. coli. This is entirely a function of cell wall morphology. E. coli is a Gram-negative bacterium, possessing a complex outer lipid membrane that acts as a robust, semi-permeable chemical shield. This barrier actively resists the influx of extreme alkalinity. Conversely, S. aureus is Gram-positive; it lacks this outer lipid envelope. Its structural peptidoglycan layer is directly exposed to the microenvironment, making it highly vulnerable to the denaturing effects of the sustained OH^- release generated by the SiO_2/C3S composite.

VI. CONCLUSION:

This study provides a comprehensive comparative analysis of SiO_2 nanoparticles, tricalcium silicate (C3S), and their physical combinations. By utilizing the Stöber and sol-gel routes, we synthesized amorphous silica and crystalline C3S structures, with their structural identities confirmed via X-ray diffraction and Raman fingerprints. Our initial optimization experiments confirmed that an 80:20 weight ratio of C3S to SiO_2 is ideal for biological deployment. This specific formulation creates a self-buffering environment that stabilizes the localized pH between 11.4 and 11.5. This managed alkalinity is strong enough to eradicate pathogenic bacteria without causing the extreme hyper-alkaline spikes (pH around 12.5) seen in pure C3S, which can damage or stress osteoblast cells. In simulated body fluid, the SiO_2/C3S composite showed exceptional biomimetic mineral growth, achieving 95% hydroxyapatite coverage within 21 days. This rapid bone-like layer formation stems from a clear chemical synergy: C3S continuously supplies the necessary Ca^{2+} ions, while the amorphous SiO_2 network offers a dense arrangement of negatively charged silanol (Si-OH) groups that act as low-barrier nucleation sites. Antibacterial monitoring over 4 and 24 hours revealed that the composite drives a potent, time-dependent destruction of Escherichia coli and Staphylococcus aureus. The composite outperformed its standalone ingredients, yielding wider inhibition zones, superior cell mortality, and a low minimum inhibitory concentration of 250 µg/mL against S. aureus. Because Gram-negative E. coli possesses a protective outer lipid membrane, it remained slightly more resilient than Gram-positive S. aureus, whose porous peptidoglycan cell wall is directly exposed to the surrounding environment. Crucially, blending the silica matrix into the silicate structure alters the hydration pathways. It breaks up the dense, impermeable calcium-silicate-hydrate passivation layer that typically chokes off pure C3S surfaces. Instead of a rapid, short-lived alkaline burst, the composite delivers a steady, long-term therapeutic ion release. Ultimately, these results mark the SiO_2/C3S platform as a highly practical, bifunctional material well-suited for simultaneous bone tissue regeneration and localized protection against bacterial infection.

ACKNOWLEDGMENT

AZS and AMP acknowledges Department of Physics, R. C. Patel Arts Commerce and Science College, Shirpur-425405, India.

Competing interests: The authors declare no competing interests.

REFERENCES

[1] S. Mou, J. Liu, C. Guo, J. Zhang, Y. Liu, X. Gao, D. Lun, and Y. Hu, "Endoprosthetic reconstruction of the diaphysis for segmental bone defects after bone tumour resection: A mid- and long-term retrospective study of 112 cases," *Bone Joint J.*, vol. 108-B, no. 2, pp. 241–250, 2026, doi: 10.1302/0301-620X.108B2.BJJ-2025-0342.R1.

[2] S. Sakdejayont, T. Chobpenthai, P. Suksirivecharuk, I.-F. Ninatkiattikul, and T. Poosiripinyo, "A review on bone tumor management: Cutting-edge strategies in bone grafting, bone graft substitute, and growth factors for defect reconstruction," *Orthop. Res. Rev.*, vol. 17, pp. 175–188, 2025, doi: 10.2147/ORR.S521832.

[3] S. Zhu, Q. Zhang, X. Xu, Z. Liu, G. Cheng, D. Long, L. Cheng, and F. Dai, "Recent advances in silk fibroin-based composites for bone repair applications: A review," *Polymers*, vol. 17, no. 6, p. 772, 2025, doi: 10.3390/polym17060772.

[4] Y. Ouyang, R. Zhang, Q. Zhang, and Y. Yan, "Polydopamine-modified composite bone cement for cancellous bone repair: Synergism

of bioactivity, antibacterial properties, and biodegradability," *Biomacromolecules*, vol. 26, no. 6, pp. 3538–3551, 2025, doi: 10.1021/acs.biomac.5c00157.

[5] N. Ab Ghani, S. Maran, M. R. Abdul Kadir, S. Somasundaram, H. R. B. Raghavendran, and T. Kamarul Zaman, "Enhancing bone grafts: Unveiling the degradation behaviour of poly(lactic-co-glycolic acid)-calcium composites for advanced bone repair," *J. Biomater. Sci. Polym. Ed.*, vol. 36, no. 11, pp. 1611–1637, 2025, doi: 10.1080/09205063.2025.2460370.

[6] E. Krishnamoorthy and B. Subramanian, "Synergistic effects of silica-enriched bioactive glass and tri-calcium phosphate nanocomposites on BMP2 gene expression for bone repair and regeneration applications," *Int. J. Pharm.*, vol. 669, p. 125026, 2025, doi: 10.1016/j.ijpharm.2024.125026.

[7] D. Wei, C. Wang, D. Ban, C. Wang, X. Liu, L. Wang, M. Chen, S. Ni, D. Song, and H. Nie, "Trace element selenium-augmented Kirschner wire with enhanced osteogenetic and antibacterial properties," *J. Mater. Sci. Technol.*, vol. 221, pp. 260–277, 2025, doi: 10.1016/j.jmst.2024.09.035.

[8] R. Talpoș-Niculescu, "Antibacterial and antifungal activity of calcium silicate-based endodontic materials: A disc diffusion study," *Farmacia*, vol. 73, no. 4, pp. 893–907, 2025, doi: 10.31925/farmacia.2025.4.9.

[9] C. Xinqi, S. Longhui, S. Huaqiao, and L. Hongwei, "Osteogenic and antibacterial effects of titanium alloy modified with copper-strontium binary doped calcium silicate coating," *Chin. J. Tissue Eng. Res.*, vol. 29, no. 22, p. 4639, 2025, doi: 10.12307/2025.464.

[10] D. Porporato, A. Luceri, E. Feyles, D. Lembo, M. Donalisio, B. Coto, S. Alves, O. Areitioaurtena, P. Persson, and C. Balagna, "Antibacterial and antiviral activities of SiO_2-Ag and ZrO_2-Ag nanocomposite coatings deposited on polymeric air filters," *Ceram. Int.*, vol. 52, no. 14, pp. 25286–25296, 2026, doi: 10.1016/j.ceramint.2026.04.139.

[11] M.-C. Lin, C.-C. Chen, I.-T. Wu, and S.-J. Ding, "Enhanced antibacterial activity of calcium silicate-based hybrid cements for bone repair," *Materials Science and Engineering: C*, vol. 110, p. 110727, 2020, doi: 10.1016/j.msec.2020.110727.

[12] J. El Hayek, H. Belaid, L. C. de Saint Cyr, G. El Chawich, E. Coy, I. Iatsunskyi, C. Gervais, J. Elango, C. Zamora-Ledezma, M. Bechelany, M. Nakhl, D. Voiry, P. Miele, M. Zakhour, L. Soussan, and C. Salameh, "3D printed bioactive calcium silicate ceramics as antibacterial scaffolds for hard tissue engineering," *Materials Advances*, vol. 5, no. 8, pp. 3228–3246, 2024, doi: 10.1039/d3ma01088k.

[13] Y.-X. Hou, H. Abdullah, D.-H. Kuo, S.-J. Leu, N. S. Gultom, and C.-H. Su, "A comparison study of SiO_2/nano metal oxide composite sphere for antibacterial application," *Composites Part B: Engineering*, vol. 133, pp. 166–176, 2018, doi: 10.1016/j.compositesb.2017.09.021.

[14] Y. Zhang, N. Imamaimaiti, X. Tang, J. Kim, T. Jiang, H. Fu, H. Pan, and Y. Wang, "SiO_2-coated ZnO for photothermal and photodynamic antibacterial applications in bone repair," *ACS Applied Bio Materials*, vol. 8, no. 6, pp. 4766–4778, 2025, doi: 10.1021/acsabm.5c00147.

[15] H. Algadi, M. Abdelfatah Alhoot, and L. A. Yaaqoob, "Systematic review of antibacterial potential in calcium oxide and silicon oxide nanoparticles for clinical and environmental infection control," *Journal of Applied Biomedicine*, vol. 23, no. 1, pp. 1–11, 2025, doi: 10.32725/jab.2025.001.

[16] D. Jana, E. Dzinovic, A. Almaroof, D. Mehta, S. Elsharkawy, S. Deb, and S. Niazi, "An in vitro study on the antimicrobial efficacy of a calcium hydroxide versus a calcium silicate-based endodontic medicament," *Clinical Oral Investigations*, vol. 29, no. 11, p. 509, 2025, doi: 10.1007/s00784-025-06524-w.

[17] K. Tsuchiya, S. Sauro, H. Sano, J. P. Matinlinna, M. Yamauti, S. Hoshika, Y. Toida, R. Islam, and A. Tomokiyo, "Clinical applications and classification of calcium silicate-based cements based on their history and evolution: A narrative review," *Clinical Oral Investigations*, vol. 29, no. 4, p. 187, 2025, doi: 10.1007/s00784-025-06274-9.

[18] S. Burhan and A. S. Mohammed, “Hydrothermal stabilization of clay soils using industrial by-products: A comprehensive review of microstructure, chemical composition, and mechanical properties,” *Environmental Earth Sciences*, vol. 84, no. 16, p. 453, 2025, doi: 10.1007/s12665-025-12452-5.

[19] Eisinas, R. Kaminskas, I. Barauskas, and L. Zinkevicius, “Synthesis and characterization of calcium silicate hydrate from biomass fly ash,” *Journal of Thermal Analysis and Calorimetry*, vol. 150, no. 2, pp. 965–975, 2025, doi: 10.1007/s10973-024-13670-y.

[20] V. Fedorova, O. N. Pestova, A. A. Selyutin, and V. L. Stolyarova, “Peculiarities of phase formation in the $Cs_2O–Al_2O_3–SiO_2$ system prepared from precursors obtained by hydrothermal synthesis,” *Russian Chemical Bulletin*, vol. 74, no. 1, pp. 58–65, 2025, doi: 10.1007/s11172-025-4499-4.

[21] M.-C. Lin, C.-C. Chen, I.-T. Wu, and S.-J. Ding, "Enhanced antibacterial activity of calcium silicate-based hybrid cements for bone repair," *Materials Science and Engineering: C*, vol. 110, p. 110727, 2020, doi: 10.1016/j.msec.2020.110727.

[22] J. El Hayek *et al.*, "3D printed bioactive calcium silicate ceramics as antibacterial scaffolds for hard tissue engineering," *Materials Advances*, vol. 5, no. 8, pp. 3228–3246, 2024, doi: 10.1039/D3MA01088K.

[23] Y.-X. Hou, H. Abdullah, D.-H. Kuo, S.-J. Leu, N. S. Gultom, and C.-H. Su, "A comparison study of SiO_2/nano metal oxide composite sphere for antibacterial application," *Composites Part B: Engineering*, vol. 133, pp. 166–176, 2018, doi: 10.1016/j.compositesb.2017.09.021.

[24] Y. Zhang *et al.*, "SiO_2-coated ZnO for photothermal and photodynamic antibacterial applications in bone repair," *ACS Applied Bio Materials*, vol. 8, no. 6, pp. 4766–4778, 2025, doi: 10.1021/acsabm.5c00147.

[25] H. Algadi, M. A. Alhoot, and L. A. Yaaqoob, "Systematic review of antibacterial potential in calcium oxide and silicon oxide nanoparticles for clinical and environmental infection control," *Journal of Applied Biomedicine*, vol. 23, no. 1, pp. 1–11, 2025, doi: 10.32725/jab.2025.001.

[26] Jana *et al.*, "An in vitro study on the antimicrobial efficacy of a calcium hydroxide versus a calcium silicate-based endodontic medicament," *Clinical Oral Investigations*, vol. 29, no. 11, p. 509, 2025, doi: 10.1007/s00784-025-06524-w.

[27] K. Tsuchiya *et al.*, "Clinical applications and classification of calcium silicate-based cements based on their history and evolution: A narrative review," *Clinical Oral Investigations*, vol. 29, no. 4, p. 187, 2025, doi: 10.1007/s00784-025-06274-9.

[28] S. Burhan and A. S. Mohammed, "Hydrothermal stabilization of clay soils using industrial by-products: A comprehensive review of microstructure, chemical composition, and mechanical properties," *Environmental Earth Sciences*, vol. 84, no. 16, p. 453, 2025, doi: 10.1007/s12665-025-12452-5.

[29] Eisinas, R. Kaminskas, I. Barauskas, and L. Zinkevicius, "Synthesis and characterization of calcium silicate hydrate from biomass fly ash," *Journal of Thermal Analysis and Calorimetry*, vol. 150, no. 2, pp. 965–975, 2025, doi: 10.1007/s10973-024-13670-y.

[30] V. Fedorova, O. N. Pestova, A. A. Selyutin, and V. L. Stolyarova, "Peculiarities of phase formation in the $Cs_2O–Al_2O_3–SiO_2$ system prepared from precursors obtained by hydrothermal synthesis," *Russian Chemical Bulletin*, vol. 74, no. 1, pp. 58–65, 2025, doi: 10.1007/s11172-025-4499-4.

[31] T. Kyotani and S. Kohara, "First sharp diffraction peak of silanol- and water-rich amorphous silica synthesized by Stöber method," *Journal of the American Ceramic Society*, vol. 109, no. 6, p. e70878, 2026, doi: 10.1111/jace.70878.

[32] S. Hui, Y. Han, and W. Yang, "Controllable preparation of thiol-modified silica particles by an optimized Stöber method," *Langmuir*, vol. 41, no. 27, pp. 18175–18183, 2025, doi: 10.1021/acs.langmuir.5c02097.

[33] H. W. Choi, S.-H. Um, and S.-H. Rhee, "Synthesis of a $Ca_3SiO_5–Ca_2SiO_4–Ca_3Al_2O_6$ cement system with rapid setting capacity by

spray-pyrolysis coupled with sol-gel method," *Journal of Biomedical Materials Research Part B: Applied Biomaterials*, vol. 107, no. 5, pp. 1440–1451, 2019, doi: 10.1002/jbm.b.34236.

[34] J. L. Montaño-Priede *et al.*, "Fabrication of monodispersed Au@SiO_2 nanoparticles with highly stable silica layers by ultrasound-assisted Stöber method," *Journal of Physical Chemistry C*, vol. 121, no. 17, pp. 9543–9551, 2017, doi: 10.1021/acs.jpcc.7b00933.

[35] W. Zhao and J. Chang, "Sol-gel synthesis and in vitro bioactivity of tricalcium silicate powders," *Materials Letters*, vol. 58, no. 19, pp. 2350–2353, 2004, doi: 10.1016/j.matlet.2004.02.045.

[36] Singh, S. Sheoran, S. Bhagwan, and S. Kadyan, "Optical characteristics of sol-gel derived $M_3SiO_5:Eu^{3+}$ (M = Sr, Ca and Mg) nanophosphors for display device technology," *Cogent Physics*, vol. 3, no. 1, p. 1262573, 2016, doi: 10.1080/23311940.2016.1262573.

[37] X. Song and A. Díaz-Cuenca, "Sol-gel synthesis of endodontic cements: Post-synthesis treatment to improve setting performance and bioactivity," *Materials*, vol. 15, no. 17, p. 6051, 2022, doi: 10.3390/ma15176051.

[38] R. S. Dubey, Y. B. R. D. Rajesh, and M. A. More, "Synthesis and characterization of SiO_2 nanoparticles via sol-gel method for industrial applications," *Materials Today: Proceedings*, vol. 2, no. 4, pp. 3575–3579, 2015, doi: 10.1016/j.matpr.2015.07.098.

[39] G. S. Henderson, G. M. Bancroft, H. W. Nesbitt, P. A. W. Dean, and M. R. Cicconi, "The high frequency Raman bands of vitreous SiO_2," *Physics and Chemistry of Glasses: European Journal of Glass Science and Technology Part B*, vol. 66, no. 2, pp. 63–68, 2025, doi: 10.13036/17533562.66.2.10.

[40] Hakamy, "Influence of SiO_2 nanoparticles on the microstructure, mechanical properties, and thermal stability of Portland cement nanocomposites," *Journal of Taibah University for Science*, vol. 15, no. 1, pp. 909–917, 2021, doi: 10.1080/16583655.2021.2011594.

[41] Hakamy, F. U. A. Shaikh, and I. M. Low, "Characteristics of hemp fabric reinforced nanoclay-cement nanocomposites," *Cement and Concrete Composites*, vol. 50, pp. 27–35, 2014, doi: 10.1016/j.cemconcomp.2014.03.002.

[42] S. Nilegave *et al.*, "Hexagonal cadmium sulfide cathode for aqueous zinc-ion battery: Study of zinc-sulfide formation and Zn/CdS battery stability," *Journal of Physical Chemistry C*, vol. 129, no. 42, pp. 18877–18886, 2025, doi: 10.1021/acs.jpcc.5c04055.

[43] D. S. Nilegave *et al.*, "Fabrication of Cu_2NiSnS_4 nanoparticles on CdS with a computationally predicted low lattice mismatch for photoelectrochemical hydrogen evolution," *ACS Applied Nano Materials*, vol. 8, no. 3, pp. 1628–1639, 2025, doi: 10.1021/acsanm.4c06654.

[44] N. Biswas *et al.*, "Phase pure, high hardness, biocompatible calcium silicates with excellent anti-bacterial and biofilm inhibition efficacies for endodontic and orthopaedic applications," *Journal of the Mechanical Behavior of Biomedical Materials*, vol. 86, pp. 264–283, 2018, doi: 10.1016/j.jmbbm.2018.06.046.